# Results of silicon pore optics mirror modules optical integration of the ATHENA telescope

G. Valsecchi*[a], F. Marioni[a], G. Bianucci[a], F.E. Zocchi[a], D. Gallieni[b], G. Parodi[c], M. Ottolini[c], M. Collon[d], G. Pareschi[e], D. Spiga[e], M. Bavdaz[f], E. Wille[f], V. Burwitz[g]
[a]Media Lario S.r.l., Località Pascolo, 23842 Bosisio Parini, Italy
[b]A.D.S. International S.r.l., via Roma 87, 23868 Valmadrera, Italy
[c]BCV Progetti S.r.l., Via S. Orsola1, 20123 Milano, Italy
[d]Cosine Research B.V, Oosteinde 36, NL-2361 HE Warmond, The Netherlands
[e]INAF Osservatorio Astronomico di Brera, Via E. Bianchi 46, 23807 Merate, Italy
[f]European Space Agency, ESTEC, Keplerlaan 1, NL-2200 AG Noordwijk, The Netherlands
[g]MPI für extraterrestrische Physik, 85748 Garching, Munich, Germany

## ABSTRACT

ATHENA (Advanced Telescope for High-ENergy Astrophysics) is the next high-energy astrophysical mission of the European Space Agency. Media Lario leads an industrial and scientific team that has developed a process to align and integrate more than 700 silicon pore optics mirror modules into the ATHENA X-ray telescope. The process is based on the ultra-violet imaging at 218 nm of each mirror module on the focal plane of a 12 m focal length optical bench. Specifically, the position of the centroid of the point spread function produced by each mirror module when illuminated by a collimated plane is used to align each mirror module. Experimental integration tests and correlation with X-ray measurement at the PANTER test facility in Münich have demonstrated that this process meets the accuracy requirement. This technique allows arbitrary integration sequence and mirror module exchangeability. Moreover, it enables monitoring the telescope point spread function during the integration phase.

**Keywords:** X-ray optics, X-ray telescopes, ATHENA, Silicon Pore Optics, Integration, Optical Alignment.

## 1 INTRODUCTION

The ATHENA (Advanced Telescope for High-ENergy Astrophysics) mission [1]-[3] of the European Space Agency is based on an X-ray telescope with a focal length of 12 m and an angular resolution of 5 arcsec half energy width (HEW). The telescope consists in a 2.5 m circular supporting structure on which about 700 Silicon pore optics (SPO) mirror modules (MM) [4] are integrated. Media Lario and a scientific and industrial team composed by ADS International, BCV Progetti, Cosine, INAF-OAB, and TAS-I have developed the process for the alignment and assembly of the 700 MMs into the ATHENA telescope within the 1.5 arcsec (1 arcsec goal) [5] error budget allocated for integration. The process has the following distinguishing characteristics:

- implementation in standard ISO 5/6 cleanroom (no vacuum infrastructure needed);
- integration of 2 MMs per day, equivalent to 2-year total integration time for the entire telescope;
- arbitrary integration sequence of the 700 MMs;
- option to remove, re-align, or replace any MM in any integration sequence scenario;
- full-telescope illumination, to monitor the optical performance during integration;
- easy telescope dismount/realign procedures for intermediate tests at X-ray facilities.

The alignment and integration concept consists in using a vertical optical bench to capture the focal plane image of each SPO MM while illuminated by a reference plane wave at a wavelength of 218 nm. The light emitted by the UV source is reflected by a parabolic mirror to generate a beam collimated to better than 45 km, thus simulating illumination from deep

giuseppe.valsecchi@medialario.com; phone +39 031 867111; medialario.com

space. The MM focuses the collimated beam onto a CCD camera placed at the 12 m focal position and the acquired point spread function (PSF) is processed in real time to calculate the centroid position and intensity parameters. This information is then used guide the robot-assisted alignment sequence.

The simplicity, precision, and accuracy of this process is based upon the fact that the intensity of the UV focal image and the position of its centroid are 1:1 proxies of the actual X-ray intensity and centroid position. This is supported by simulations and confirmed by X-ray measurements at the PANTER test facility [6] in Münich. *De facto*, we have extended to silicon pore optics the proven mirror modules integration heritage used in all major X-ray missions, from Beppo-SAX to XMM-Newton and eROSITA [7].

In this paper, we describe in detail the integration procedure and the results on the integration demonstration performed on a mock up structure in which 2 MMs have been assembled. The correlation between the measurements done at UV and X-ray at the PANTER test facility are also reported.

## 2 INTEGRATION FACILITY

The optical bench is schematically shown in Figure 1, left. The light source is a broadband incoherent lamp from Energetiq, with a diverging beam that illuminates a 5.0 m focal length, 780 mm diameter, parabolic collimator through a 50 µm pinhole, which corresponds to a 4.5 arcsec at the focal plane. The light is reflected by the parabolic mirror into a plane wave, collimated better than 45 km. The incident plane wave is then focused by the SPO MM on a CCD at 12 m. The broadband light is filtered at the focal plane by a 20 nm bandpass filter centred at 218 nm. The source power in this bandwidth is of the order of few nanowatt. The CCD camera, from Princeton Instruments, has 1024×1024 square pixels of 13 µm in side. We use a 2×2 pixels binning strategy, resulting in an effective pixel size of 26 µm corresponding to a field of view of 0.45 arcsec over a focal length of 12 m.

A robotic device manipulates the MM over the mirror structure in all 6 degrees of freedom. This robotic handler has been designed and realized to validate the concept of semi-automatic loading, placement, and fine alignment of the MM at their respective locations across the entire X-ray telescope. In this project, the robotic handler has been realized with a travel range limited a small area. However, all the features of the machine are representative of a full-scale unit and have allowed us to exercise and test all the capabilities of this device. In its full-scale implementation, the robotic handler will provide:

- fine positioning and orientation of any MM of any row and azimuth;
- accessibility in the narrow gaps between MMs of different rows;
- magnetic pick-and-place of any MM designs, i.e. different sizes for different rows;
- native RX and RY (rotation around X and Y axis) fine-alignment capability;

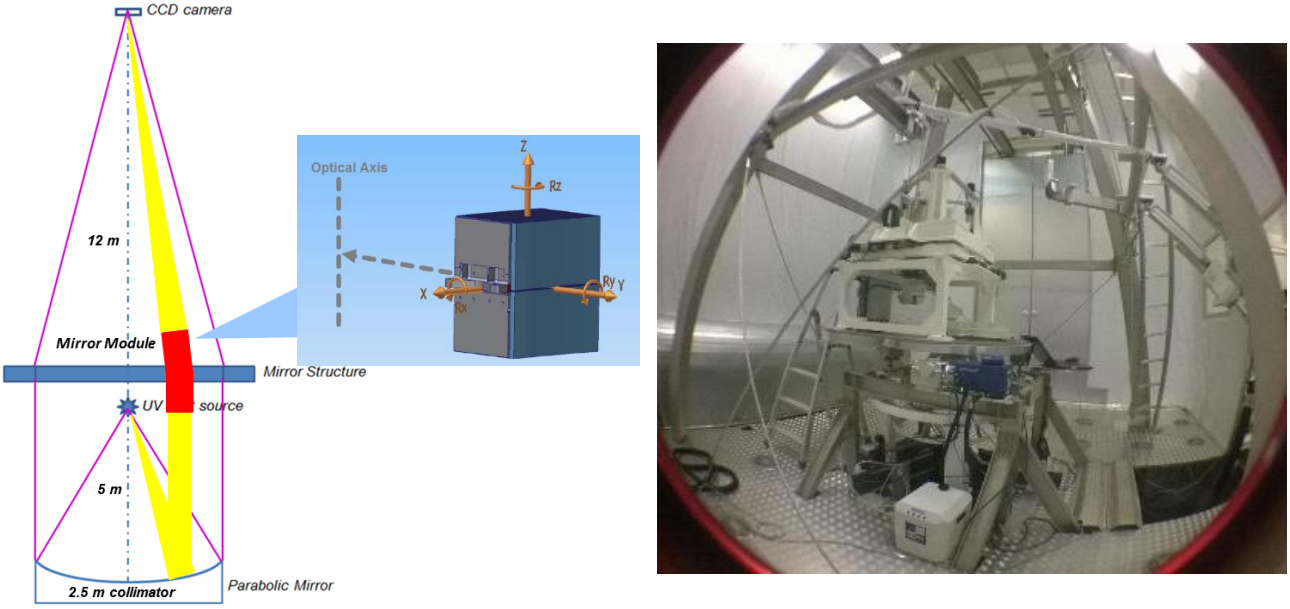


Figure 1. Schematic illustration of the alignment setup for the MM (left) and a picture of the actual optical bench (right).

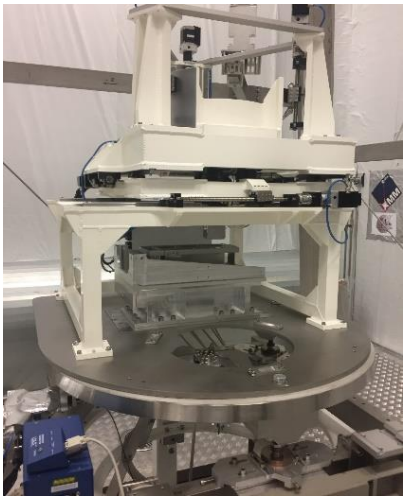

| Positioning | Range | Accuracy |
|---|---|---|
| X translation | ±100 mm | ±1.3 µm |
| Y translation | −25 ÷ +90 mm | ±1.3 µm |
| Z translation | 120 mm | ±10 µm |
| X rotation | ± 2° | ±20 arcsec |
| Y rotation | ± 2° | ±80 arcsec |
| Z rotation | 360° | ±3.2 arcsec |

Figure 2. The robotic handler mounted on the optical bench (left) and positioning range and accuracy (right).

The robotic handler is mounted on the optical bench as shown in Figure 2 and provides accurate control of the MM in all its six degrees of freedom, as detailed in the table. The X, Y, Z axis are controlled by seven linear stages with recirculating ball screws driven by stepper motors. The rotation $R_Z$ around the optical axis Z is controlled by a fully-steerable 360° rotator mounted on a custom worm-wheel coupled to a precision and ultra-thin-section bearing.

$R_X$ (azimuth) and $R_Y$ (radius) are more complex because they occur around a virtual pivot in the centre of the mirror module. $R_X$ is created by a set of properly arranged flexures so that the stage holding the MM is pre-loaded by a central spring against a stepper linear actuator. The pre-loading force covers about one half of the force budget of the linear actuator. The linear actuator produces a rotation about the virtual pivot axis. $R_Y$ is achieved by means of a swinging platform featuring two guiding arches with a unique axis of rotation. This approach produces a stiff rotation axis projected far beyond the physical mechanical stage.

## 3 MIRROR MODULE ALIGNMENT AND INTEGRATION

The SPO mirror module consists of two silicon plate stacks, each with an array of square channels (or pores) measuring 0.83 mm × 0.83 mm (typical). The stacks are arranged in Wolter-like configuration, each pore being a double-reflection grazing incidence focusing system. The illumination at 218 nm creates a diffraction pattern with a period of of $\lambda/d \cong 54$ arcsec [8]. The optical path is the same for all the pores of each row over the entire 360° azimuth, whereas it changes for different rows, so that the interference occurring among the rays of each row creates the diffraction pattern of Figure 3, where the azimuth direction corresponds to the horizontal direction on the page. Simulated and measured images show a perfect match, as shown in Figure 3.

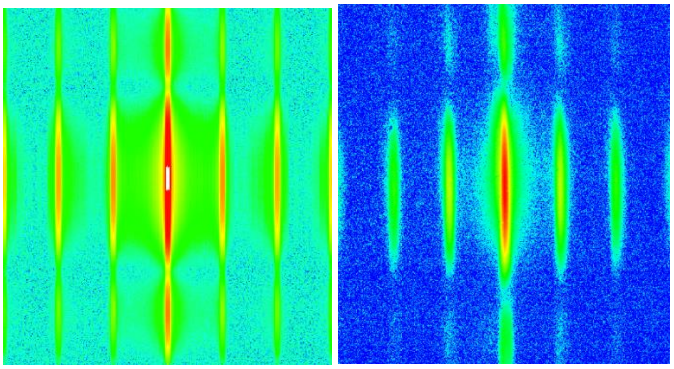

Figure 3. Simulated (left) and measured (right) diffraction patterns from MM with 218 nm illumination (images with logarithmic scale).

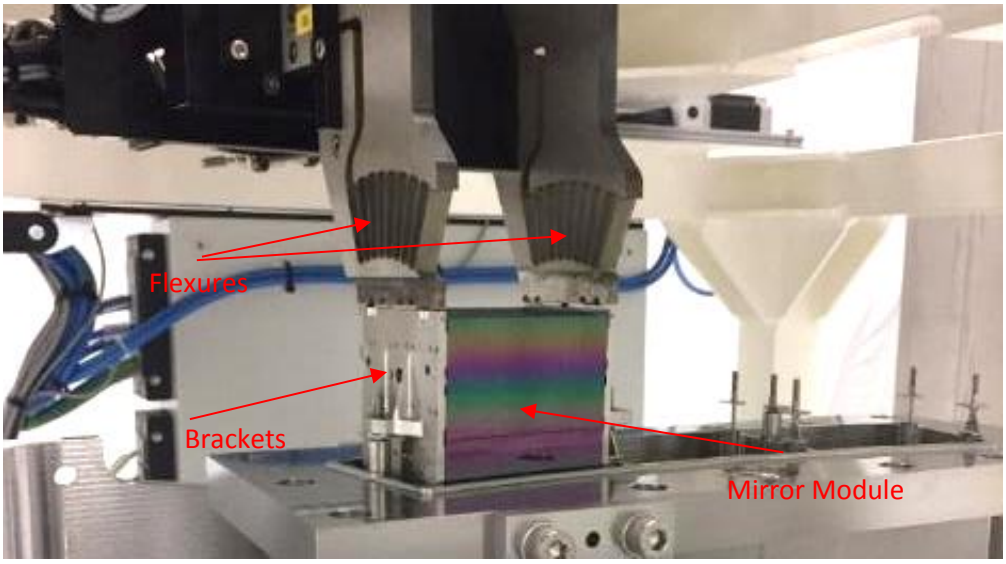


Figure 4. Flexures of the robotic handler holding the MM from the brackets through small magnets.

### 3.1 Alignment and integration sequence

The MM alignment consists of three steps that determine the best orientation of the MM in all its six degrees of freedom illustrated in Figure 1. The alignment is guided by specific parameters calculated from the 218 nm MM focal plane image acquired by the CCD camera [9]:

- maximization of photon count, for rotation $R_X$ and $R_Y$ around X and Y, respectively;
- the position of the image centroid, for rotation $R_Z$ around Z and displacements $\Delta X$ and $\Delta Y$ along X and Y;
- mechanical reference, for displacement $\Delta Z$ along the optical axis Z.

The robotic handler is used to move and align the MM over the correct position of the mirror structure. The robotic handler holds the MM with two calibrated flexures that have three small magnets to hold the MM from the Invar brackets (two flanges attached to the MM for handling and integration), as shown in Figure 4.

In more detail, the first step of the process is the alignment of the MM in tip ($R_X$) and tilt ($R_Y$) until the intensity of the focal plane image is maximum. A series of images are acquired at different tip/tilt positions of the MM and their intensity values (i.e. photon count) are plotted as function of the tip/tilt values (Figure 5). The best tip/tilt position is at the maximum of each plot, that is the position with minimum vignetting.

The second step is the alignment of the MM in rotation ($R_Z$) and azimuthal position ($\Delta X$), which cause exclusively an X displacement of the centroid. First, the X position of the MM is set so that the dowel pins are approximately centred in the slot holes of the MM bracket. Then the MM is rotated around the Z axis until the centroid is aligned to the X = 0 coordinate of the CCD. This step ends with the alignment of the MM in the azimuthal position $\Delta Y$ until the centroid of the MM is exactly at the centre of the focal plane, as shown in Figure 6.

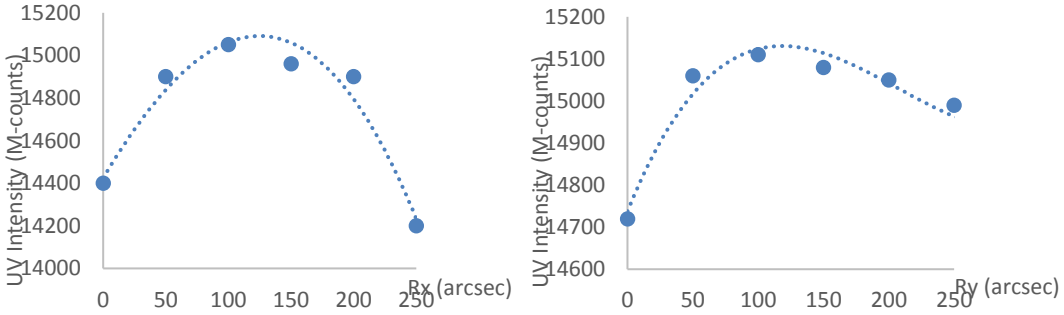


Figure 5. Tip ($R_X$) and tilt ($R_Y$) alignment optimization of the MM.

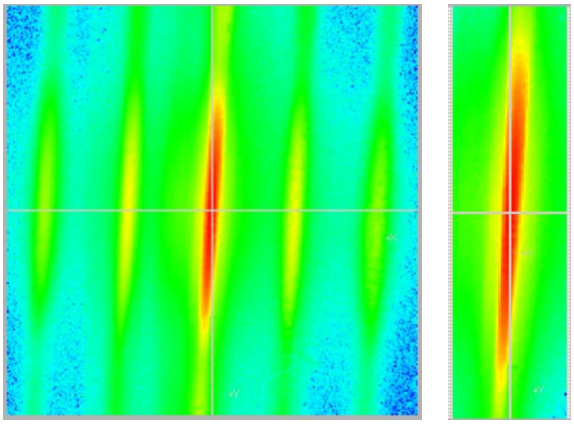

Figure 6. PSF image (left) and area for centroid calculation (right) of aligned MM.

The vertical alignment (ΔZ) is adjusted with mechanical reference. First the MM is lowered to touch the dowel pin surface and then it is raised by 100 µm. An electric grounding check between the MM and the Mirror Structure is used to determine the mechanical contact between the brackets and the dowel pins. This mechanical alignment procedure is enough because the HEW is very insensitive to the vertical position of the MM.

After alignment, the MM is integrated to the mirror structure through the dowel pins, which have previously been bonded to the mirror structure. The dowel pins act as mechanical interfaces between the MM and the mirror structure (Figure 7). After alignment, the MM is in a position in which the top heads of the dowel pins are in the slot holes of the MM brackets. The lateral clearance between the dowel pins and the brackets holes is approximately 0.25 mm, sufficient for the alignment range of the MM. The vertical clearance between the flat shelf of the dowel pins and the corresponding area of the brackets is 0.1-0.2 mm, which is the bonding area for the MM integration. The electric grounding check ensures that there is no mechanical contact between the brackets and the dowel pins.

The top part of the dowel pins has a 0.8 mm channel with two orifices in correspondence of the flat shelf of the pin. While the MM is held in its best alignment position by the robotic handler, a controlled amount of epoxy adhesive is injected in the channel to fill, by capillary action, the gap between the bracket and the flat shelf of the pin (Figure 7). The epoxy adhesive has the right viscosity for an effective capillary action. Moreover, its low-shrinkage characteristics do not impact the alignment during the 12 hr, room-temperature curing process, as we have experimentally verified on the optical bench. After curing, the robotic handler is detached from the MM and available for the alignment of the next MM.

### 3.2 Comparison between ultraviolet and X-ray measurements of single mirror modules

To confirm that the UV centroid is a 1:1 proxy of the corresponding X-ray centroid, we extensively characterized both centroids at our optical bench and at the PANTER test facility. The MM has been provided by the European Space Agency and Cosine, and it consists of parabolic-hyperbolic stacks with 34 plates. The MM has 65 pores distributed over its width with a constant 1 mm pitch, so that the pores measure 0.83 mm in width and 0.606 mm in height. The plates are co-focal

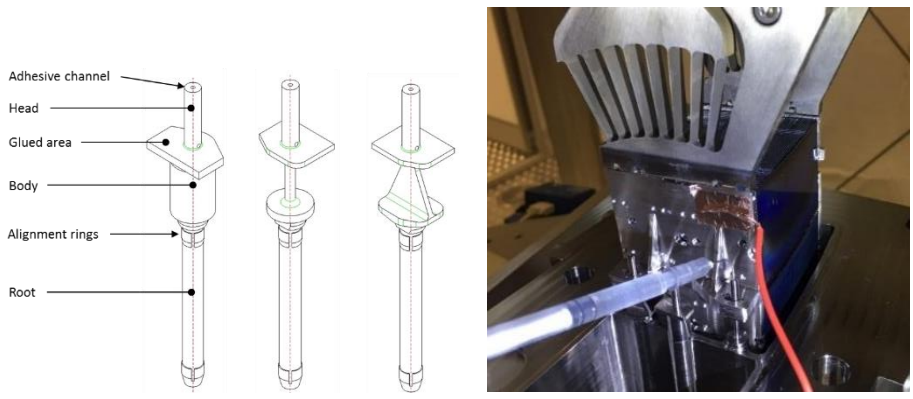


Figure 7. Interface area between the brackets and dowel pins (left) and injection of the epoxy adhesive for the final integration of the MM (right).

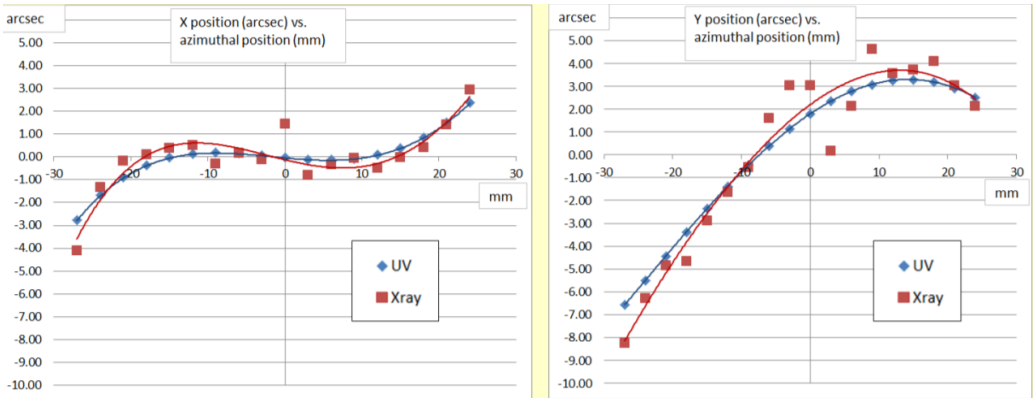


Figure 8. Comparison of UV and X-ray centroid position.

and their profile is wedged, hence the incidence angle increases by 2.1 arcsec from one plate to the next.

Focal plane images have been acquired for twenty separate MM sections along the azimuthal direction, and the corresponding centroids have been calculated from the main lobe of the diffraction pattern. The same measurements have been repeated at the PANTER test facility at 1.49 keV (Aluminum $k_\alpha$ line) . The correlation between UV and X-ray metrology has been verified by plotting the azimuthal (horizontal) and radial (vertical) centroid shifts as a function of the position of the illuminated MM section (Figure 8). The standard deviation of the position difference of the UV and X-ray centroids is 0.38 arcsec along azimuth and 0.61 arcsec along radius against an allocated budget of 0.25 arcsec. The result is promising, and there is ample margin of improvement in the measurement setups, as follows:

- UV measurement illuminated the entire MM, whereas only about 50% of each pore was illuminated at X-ray because of the finite source distance (120 m);
- the optical bench has been improved with more powerful (15x) and more stable (25x) UV source, a more efficient CCD camera, and higher efficiency mirror coating;
- the MM test vehicle was an initial experimental unit with HEW of 15-40 arcsec.

# 4 ALIGNMENT ERROR BUDGET

## 4.1 Error budget of alignment of single mirror module

The robustness of the alignment procedure is supported by extensive ray-tracing simulations at X-ray and UV wavelengths. The main driver for the definition of the alignment metrology and procedure and for the design of the telescope structure is the error budget for the angular resolution of the ATHENA telescope, as set by the Agency (Table 1). The integration of about 700 MMs has a total allocated error budget of 1.5 arcsec (goal 1 arcsec). We have further broken this global error value into individual MM, which has then become the main performance driver for the metrology and integration process. We have assumed the following simplified one-dimensional model:

1. all MMs have the same PSF on the telescope focal plane;
2. the PSF of each MM is described by a one-dimensional Gaussian function;
3. the effective area is the same for all MMs;
4. the distribution of the alignment error is a one-dimensional Gaussian function.

Table 1. HEW error budget for the ATHENA telescope.

| **HEW telescope error budget** | **Requirement [arcsec]** | **Goal [arcsec]** |
|---|---|---|
| Mirror Module | 4.3 | 2.5 |
| Alignment and integration | 1.5 | 1.0 |
| Distortions | 1.5 | 1.0 |
| Spacecraft related | 1.0 | 0.5 |
| Margin | 1.0 | 0.5 |
| **Root Square Sum** | **5.0** | **3.0** |

Table 2. Ray-tracing simulation of the telescope HEW using a 2D Gaussian distribution of the centroids position errors.

| HEW of individual MM [arcsec] | 1σ MM integration error [arcsec] | HEW of the telescope [arcsec |
|---|---|---|
| 3.5 | 1 | 3.9 |
| | 2 | 4.3 |
| 4 | 1 | 4.4 |
| | 2 | 5.1 |

The effect of the MMs alignment errors is simulated by the centroid shift of each MM, described with a one-dimensional Gaussian distribution with standard deviation $\sigma$. The total PSF is the convolution of the PSF of the MMs with their centroid shifts, both described by one-dimensional Gaussian distributions. The convolution is also a Gaussian function with variance equal to the sum of the variances of the two original Gaussian functions. Therefore, the HEW of the entire telescope is given by

$$\mathrm{HEW}_{\mathrm{Population}} = \sqrt{\mathrm{HEW}_{\mathrm{MM}}^2 + (1.349\sigma_{\mathrm{centroids}})^2}$$

where 1.349 is the ratio between the HEW and the standard deviation for a one-dimensional Gaussian function. Since the goal for the HEW of each MM is 2.5 arcsec and 1 arcsec is allocated in quadrature for the MMs alignment and integration error, the HEW of the entire integrated MM population is 2.7 arcsec. Consequently, the $\sigma$ of the distribution of the centroids after integration must be smaller than

$$\sigma_{\mathrm{centroids}} \leq \frac{1}{1.349}\sqrt{\mathrm{HEW}_{\mathrm{Population}}^2 - \mathrm{HEW}_{\mathrm{MM}}^2} = \frac{1}{1.349} = 0.74 \text{ arcsec}$$

Therefore, 0.74 arcsec is the error budget (standard deviation) allocated to each individual MM in order to meet the 1 arcsec error budget goal for the entire population of ≈700 MMs. To further support our analysis, we have verified the one-dimensional assumption 4 above by raytracing of two-dimensional Gaussian distribution of the position errors of the centroids. The results (Table 2) closely match the simplified approach.

Table 3. Sub-system integration error budget for the demonstrator and for the FM (X, Y, Z correspond to azimuthal, radial and optical axis coordinates).

| Sub System | Parameter | Demonstrator | Flight module |
|---|---|---|---|
| Telescope integration | HEW | < 1.5 arcsec | < 1.5 arcsec |
| | Effective area loss | < 5% | < 1% |
| MM accuracy | Accuracy of MM focal length | < 5 mm | < 1.5 ÷ 2.5 mm |
| | X and Y alignment accuracy of brackets | < 0.5 mm | < 0.5 mm |
| MM alignment | Maximum X and Y errors | < 12 μm | < 12 μm |
| | Maximum $R_X$ error | < 100 arcsec | < 10 ÷ 30 arcsec |
| | Maximum $R_Y$ error | < 400 arcsec | < 30 ÷ 120 arcsec |
| Optical bench | Collimation of UV illumination beam | > 41 km | > 95 km |
| | Collimation stability | > 41 km | > 1500 km |
| | Z position accuracy of the source | < 160 μm | < 380 μm |
| | Z position stability of the source | < 160 μm | < 23 μm |
| | Z position accuracy of the CCD camera | < 3.5 mm | < 1.5 mm |
| | Z position stability of the CCD camera | < 3.5 mm | < 93 μm |
| | $R_Z$ stability during curing | < 3.2 arcsec | < 1.5 ÷ 9 arcsec |

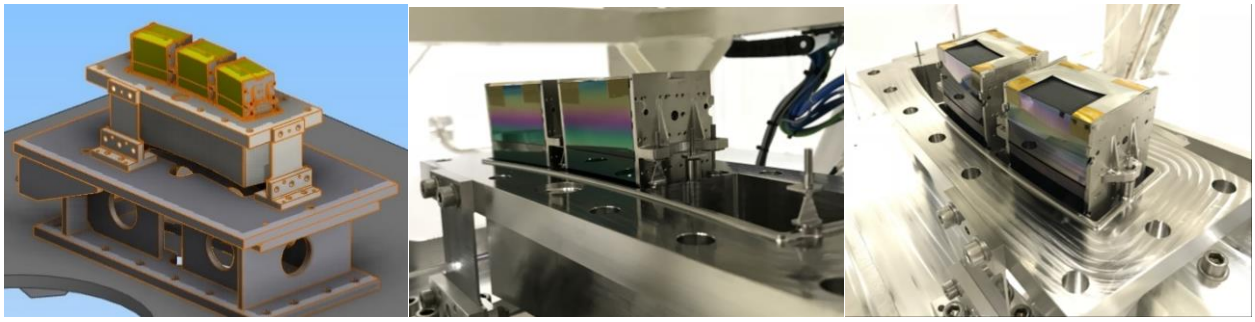

Figure 9. Demonstrator design (left) and build (centre, right) with two SPO MMs aligned and integrated on the mirror structure element.

### 4.2 Subsystem and component level specifications

A set of lower level specifications for the main subsystems and components has been derived from the high-level telescope requirements. They include the alignment tolerance of the mirror modules, the accuracy and stability of the optical bench and the optical performance of the mirror modules. This set of requirements is summarized in Table 3 for both the demonstrator and, preliminarily, the flight module.

## 5 INTEGRATION DEMONSTRATOR

This alignment and integration process and its associated metrology and facility have been experimentally verified on a representative ATHENA telescope demonstrator. The demonstrator consists of two SPO MMs integrated in a mirror structure element (MSE) that is an exact cut-out of row 8 of the ATHENA telescope mirror structure (Figure 9). The MSE is made of Titanium and can accommodate up to three MMs spaced by 7.25° in azimuth. The MSE is fixed to an additional support by means of three flexures so that it can be shaken and thermal tested so that the MMs are loaded with the typical ATHENA mission loads. First, we have aligned and bonded MMs #0025 and #0027 in the MSE, followed by X-ray tests at PANTER. Then we have removed, re-aligned and re-integrated the MM #0025 to demonstrate that our process allows the removal and replacement of any MMs at any telescope population stage. The demonstrator has then been again tested at PANTER.

The measurements at the PANTER test facility in Münich has been performed at 1.49 keV to confirm the achieved alignment tolerance. The main objective of the test is the alignment and integration of the MMs at the x-FWHM (i.e. azimuthal FWHM) focal length, where the transversal PSF performance is only few arcseconds. This decision has been taken after analyzing the X-ray characterization of the individual MMs done at the X-ray beam line of the Bessy II facility [10]. In fact, both MMs have best transversal PSF at a focal length of 11,963 mm, instead of the nominal 12,000 mm, whereas the best HEW was considerably larger than the FWHM and with a focal length 50-60 mm shorter. HEW and FWHM measured at the nominal focal length are shown in Table 4.

Figure 10 shows the UV and X-ray images of the resulting PSF, with clearly visible overlapped centroids. Figure 11 shows the X-ray HEW (top), x-FWHM (middle) and the centroid distance (bottom), all plotted against the focal distance.

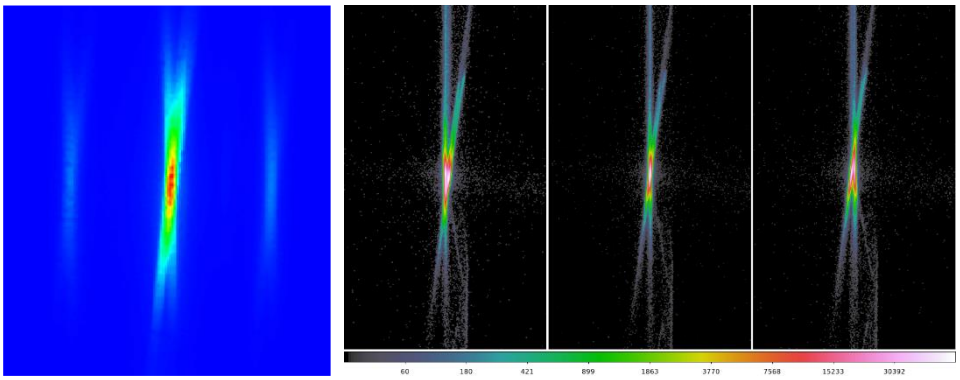


Figure 10. Demonstrator PSF at 218 nm (left) and at 1.49 keV at intra, nominal, and extra focal positions (right).

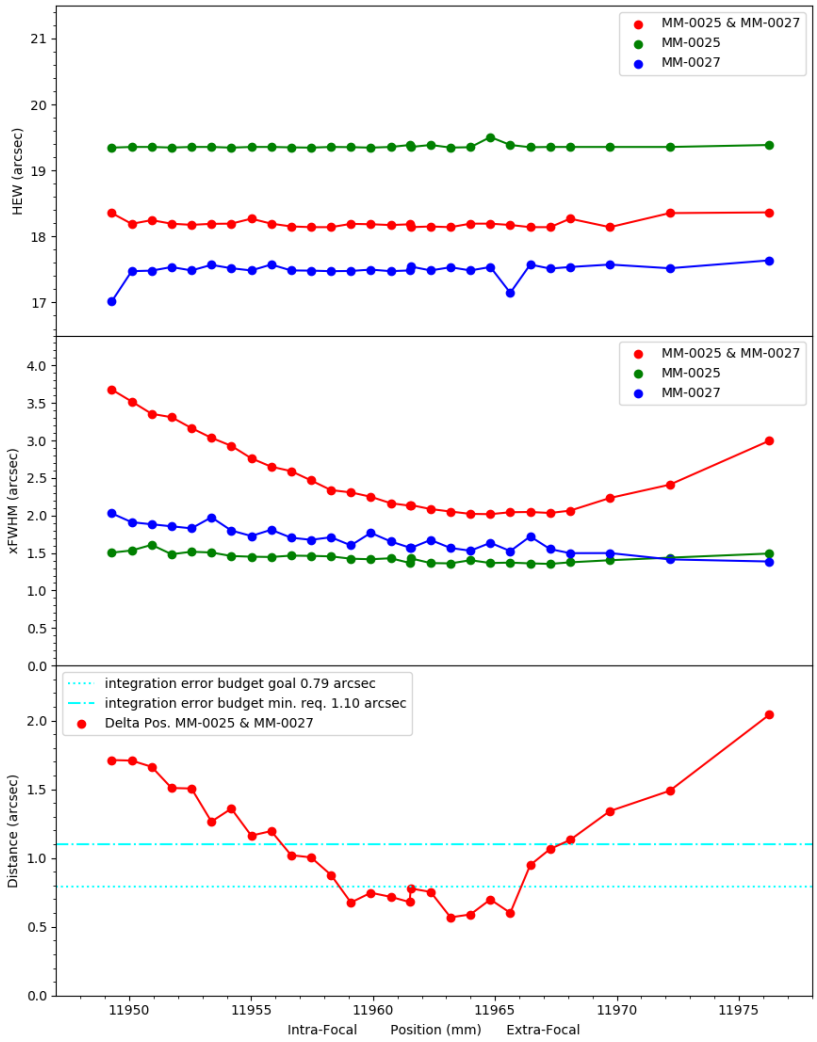


Figure 11. From top to bottom, X-ray HEW, x-FWHM (azimuthal), and distance between the two centroids plotted as a function of the focal distance.

In particular, the bottom graph of Figure 11 showing the difference between the positions of the two MM centroids plotted as a function of the focal distance, confirms that the two MMs have been integrated at their best focal distance of 11,963 mm where the distance between the centroids' positions is the smallest. This difference is 7 µm in X and 36 µm in Y, for a total distance of. 36.6 µm. Since at PANTER the optics is positioned at the finite distance of 120 m from the point source, the effective focal length of the MMs increases from the nominal 11,963 mm to 13,270 mm. Consequently, the position difference of 36.6 µm between the centroids of the 2 MMs corresponds to 0.57 arcsec, well within the allocated budget of 0.74 arcsec discussed in Section 4.

Finally, it should be underlined that MM #0025 has been disassembled from the MSE, cleaned, re-aligned, and bonded again to the same housing of the MSE, as per agreed test plan, without any optical degradation or variation, thus demonstrating the remove-and-replace capability of MMs of the integration process.

Table 4. FWHM results of the 2-MM Integration Demonstrator.

| **Optical element** | **Focal length** | **FWHM** | **HEW** |
|---|---|---|---|
| MM #0025 | 11,963 mm | 1.4 arcsec | 19.3 arcsec |
| MM #0027 | 11,963 mm | 1.6 arcsec | 17.5 arcsec |
| MM #0025 + MM #0027 | 11,963 mm | 2.0 arcsec | 18.1 arcsec |

## 6 CONCLUSIONS

Media Lario and the team of scientific and industrial partners have developed the process for the alignment and integration of about 700 silicon pore optics mirror modules in the 2.5 m diameter structure of the X-ray ATHENA telescope.

The process has been implemented at the Medial Lario 12 m focal length optical bench and a representative demonstrator with two silicon pore optics mirror modules has been successfully integrated. The distance between the position of the centroids of the two mirror modules has been measured at X-ray wavelength at the PANTER test facility in 0.57 arcsec, with no changes after removal and re-integration of one MM. This is well within the 0.74 arcsec goal derived, for each individual MM alignment, from the overall telescope alignment and integration budget of 1 arcsec.

## ACKNOWLEDGMENT

This work has been done in the framework of the European Space Agency contract 4000114931/15/NL/HB.

## REFERENCES

[1] ESA, 2ATHENA: Assessment of an X-Ray telescope for ESA Cosmic Vision Program," CDF-150(A) (2014).
[2] <http://www.the-athena-x-ray-observatory.eu>.
[3] <http://sci.esa.int/cosmic-vision/54517-athena>.
[4] Collon, M.J., Vacanti, G., Günther, R., Yanson, A., Barrière, N., et al., "Silicon pore optics development for ATHENA," Proc. SPIE 9603, (2015).
[5] Ayre, M., Bavdaz, M., Ferreira, I., Wille, E., Fransen, S., Stefanescu, A., Linder, M., "ATHENA – System studies and optics accommodation," Proc. SPIE 9905, 990526 (2016).
[6] <http://www.mpe.mpg.de/heg/panter>.
[7] Burwitz, V., Predehl, P., Friedrich, P., Bräuninger, H., Eder, J., et. al., "The calibration and testing of eROSITA X-ray mission assemblies," Proc. SPIE 9144, (2014).
[8] Spiga, D., Collon, D.M., Conconi,P., Valsecchi, G., Wille, E., et al., "Optical simulations for design, alignment, and performance prediction of silicon pore optics for the ATHENA X-ray telescope," Proc. SPIE 10399-16 (2017).
[9] Valsecchi, G., Marioni, F., Bianucci, G., Zocchi, F.E., Gallieni, D., Parodi, G., Ottolini, M., Collon, D.M., Pareschi, G., Spiga, D., Bavdaz, M., Wille E., et al. "Optical integration of SPO mirror modules in the ATHENA telescope," Proc. SPIE 10399-13 (2017).
[10] <https://www.helmholtz-berlin.de/quellen/bessy/index_en.html>